Novel Compact Model for the Radiation Pattern of UWB Antenna using Vector Spherical and Slepian Decomposition

Wouter Dullaert, Hendrik Rogier, *Senior Member IEEE*

Abstract

In this paper a new compact model to describe the 3D radiation pattern of an Ultra Wideband antenna, using a Vector Spherical and Slepian decomposition, is presented. Vector Spherical modes are known to provide a good basis for the angular dependency of the radiation pattern. This paper is the first to extend such a model to also incorporate the frequency dependency of a radiation pattern. This is achieved by using a Slepian mode expansion. It is shown that this model requires considerably less coefficients than traditional sampling to accurately describe a frequency-dependent 3D radiation pattern. Also, generating the Slepian modes is computationally more efficient than comparable techniques, such as the Singularity Expansion Method (SEM). The coefficients can then directly be used to efficiently calculate performance measures such as the antenna Fidelity Factor for all angles (ϕ, θ) without reconstructing the radiation pattern, or to reduce the noise contribution.

Index Terms

Antenna Radiation Patterns, Ultrawideband Antennas, Ultrawideband Radiation, Modeling, Fidelity Factor, DPSS, Spherical Modes

I. Introduction

Ultra Wideband (UWB) communication is a very hot topic at the moment in both industrial and academic research. The protocol already exists for quite some time in military radar applications, but since the frequency band allocation by the FCC in 2002, [1], interest for consumer applications gained momentum. In [1] a UWB system is defined as a communication system that has an absolute bandwidth larger than 500 MHz or a relative bandwidth larger than 0.2 times the center frequency. The FCC allows unlicensed use of these systems between 3.1 GHz and 10.6 GHz with a spectral mask of -41.6 dBm. In this paper a special form of UWB communication will be used: pulse modulated UWB. It is assumed that the pulse uses the entire FCC band.

The large bandwidth, in combination with the fact that pulse modulated UWB operates in time domain, is a big challenge for the predominantly small-band and frequency-domain oriented antenna design. [2] shows that pulse distortion deserves special care when designing a UWB antenna. Unfortunately pulse distortion does not translate to traditional antenna performance measures such as return loss or gain in a straightforward manner. Therefore various performance measures for UWB antennas have been presented in literature: [3] proposed the fidelity factor, which correlates the applied voltage pulse with the pulse shape of the transmitted electric field.

In this paper, for the first time, this factor is evaluated for each pair (ϕ, θ) of azimuth and elevation angles. [4] defined the pulse width stretch ratio, which measures how much a pulse gets smeared out in time by the antenna. [5] extended the fidelity factor by replacing the applied voltage pulse in the correlation by a template function that is tailored to the situation. Finally [6] combines previous research on the Pattern Stability Factor and Pattern Stability Bandwidth.

All these performance measures require full knowledge of the frequency response of the antenna, which is closely related to the frequency-dependent radiation pattern. For an antenna covering the entire FCC band this is an impractically large amount of data. An efficient, compact representation of the radiation pattern will decrease the calculation time and the memory requirements when determining antenna performance measures.

In this paper such an efficient model is presented. As in [7], the angular dependency of the radiation pattern is modeled using a decomposition into vector spherical modes. The frequency dependency is expanded into a series of Slepian modes, which are known to be a good set of basis functions for bandlimited signals, [8]. The performance of this Slepian expansion is compared to a vector fitting technique: the singularity expansion method (SEM). Another model based parameter estimation technique is discussed in [9].

The decomposition of the radiation pattern into vector spherical modes is discussed in Section II. Section III provides some theoretical background for the Slepian expansion. In Section IV this knowledge is applied to decompose the frequency dependency of the radiation pattern into Slepian modes. The model is then used to evaluate the fidelity factor in Section V. Section VI briefly introduces the SEM technique, used for validation. In Section VII the model is validated by applying it to an in-house developed antenna and comparing the results to those obtained with the SEM method.

II. Vector Spherical Decomposition

Because of the very large bandwidths considered, the radiation pattern of an Ultra Wideband antenna must be described as a function of three variables: the azimuth angle ϕ, the elevation angle θ and the frequency f. Adding the frequency variable to the standard angular ϕ and θ variables easily increases the amount of required sample points by a factor of 50.

In this paper a full 3D radiation pattern $\boldsymbol{F}(\phi, \theta, f)$ is considered. In a first step the 3D radiation pattern $\boldsymbol{F}(\phi, \theta, f)$ is decomposed into a series of vector spherical modes. Vector spherical modes are a combination of phase modes, described in [10], and spherical modes, described in [11]. Other ways to efficiently describe the angular dependency of a radiation pattern, such as [12], have been presented, but will not be covered further. [13] and [7] show that the decomposition on the vector spherical modes results in a very compact description of the angular dependencies of the radiation pattern. In [14] this decomposition is applied to a UWB radiation pattern.

The Vector Spherical decomposition of the 3D radiation pattern $\boldsymbol{F}(\phi, \theta, f)$ is given by:

$$\boldsymbol{F}(\phi,\theta,f) = \sum_{n=1}^{+\infty} \sum_{m=-n}^{n} A_{n,m}(f)\boldsymbol{\Psi}_n^m(\phi,\theta) + B_{n,m}(f)\boldsymbol{\chi}_n^m(\phi,\theta) \tag{1}$$

Where $\boldsymbol{\Psi}_n^m(\phi,\theta)$ and $\boldsymbol{\chi}_n^m(\phi,\theta)$ are the harmonic vector spherical basis functions defined by:

$$\boldsymbol{\Psi}_n^m(\phi,\theta) = \frac{Ne^{jm\phi}}{\sqrt{n(n+1)}}\left(j\frac{d}{d\theta}P_n^m(\cos\theta)\boldsymbol{u}_\theta - \frac{mP_n^m(\cos\theta)}{\sin\theta}\boldsymbol{u}_\phi\right) \tag{2}$$

$$\boldsymbol{\chi}_n^m(\phi,\theta) = \frac{-Ne^{jm\phi}}{\sqrt{n(n+1)}}\left(\frac{mP_n^m(\cos\theta)}{\sin\theta}\boldsymbol{u}_\theta + j\frac{d}{d\theta}P_n^m(\cos\theta)\boldsymbol{u}_\phi\right) \tag{3}$$

with P_n^m representing the associated Legendre polynomials, $-n \leq m \leq n$ and N given by:

$$N = \sqrt{\frac{2n+1}{4\pi}\frac{(n-m)!}{(n+m)!}} \tag{4}$$

[7] showed that the amount of relevant phase modes, and thus by extension vector spherical modes, is limited by the dimensions of the antenna. This allows us to truncate the series by limiting the first summation in (1) to M instead of ∞. [13] suggests that this truncated series is a good approximation for the radiation pattern if $M \gg k_0 d$, with d the largest dimension of the antenna and k_0 the wave number of the highest considered frequency.

III. PSWF AND DPSS THEORY

In this section, some properties are described of the Prolate Spheroidal Wave Functions (PSWF) and the Discrete Prolate Spheroidal Sequences (DPSS), the discrete counterpart of the PSWF. There is no closed-form analytic expression known for either of them, which makes them rather difficult to generate. However, as is explained later on, they can be generated efficiently by calculating the eigenvectors from a carefully constructed matrix. They form the mathematical basis of the Slepian decomposition discussed in Section IV. For more information, the interested reader is referred to [15].

Driven by the mathematical, but unnatural, certainty that a non-trivial function cannot have limited support in both time and frequency domain, the zeroth-order PSWF $S_{0,c}(t)$ is defined as the solution to the following maximisation problem, for bandlimited $f(t)$:

$$\max \frac{\int_{-t_0}^{t_0} |f(t)|^2\, dt}{\int_{-\infty}^{\infty} |f(t)|^2\, dt} \tag{5}$$

where t_0 denotes the considered time-interval of the PSWF. The first-order PSWF $S_{1,c}(t)$ is the solution to (5) for all W-bandlimited $f(t)$ orthogonal to $S_{0,c}(t)$, where orthogonality is defined using the standard L2-norm. The higher-order PSWFs are defined in a similar fashion, [16], [17], [18], [19]

Some mathematical manipulation on (5) shows that the PSWFs are also the eigenfunctions of the sinc-kernel:

$$\int_{-1}^{1} \frac{sin(c(f-t))}{\pi(f-t)} S_{k,c}(t)dt = \lambda_{k,c} S_{k,c}(f) \tag{6}$$

where $|f| \leq 1$, $c = Wt_0$ the time-bandwidth product, W the bandwidth of $f(t)$ and $k = 0, 1, 2, ..$ is the order of the PSWF, resulting in a second way to define the PSWFs.

The PSWFs are also the solution to the following second-order differential eigenvalue problem:

$$\frac{d}{df}\left(1 - f^2\right)\frac{dS_{k,c}}{df} + \left(\chi_k - c^2 f^2\right) S_{k,c} = 0 \tag{7}$$

where χ_k is a real and positive eigenvalue: $0 < \chi_0 < \chi_1 < \ldots$. This is the third and final way to define the PSWFs. Whereas the first method is the most intuitive one, this last method gives much more information about the functions.

PSWFs form a complete and orthonormal basis for all W-bandlimited functions $f(t)$, they are orthonormal on the real time-axis and orthogonal over $[-t_0, t_0]$. The finite-Fourier transform of a PSWF satisfies:

$$\int_{-t_0}^{t_0} S_{k,c}(t)\exp(j2\pi ft)dt = j^k \left(\frac{2\pi\lambda_{k,c}t_0}{W}\right)^{1/2} S_{k,c}\left(\frac{2\pi t_0}{W}f\right) \tag{8}$$

whereas their Fourier transform satisfies:

$$\int_{-\infty}^{\infty} S_{k,c}(t)\exp(j2\pi ft)dt = j^k \left(\frac{2\pi t_0}{W}\right)^{1/2} S_{k,c}\left(\frac{2\pi t_0}{W}f\right) \tag{9}$$

Because of the numerous properties associated with these functions, they have been used in a multitude of different fields. [20] proposed to use them as the basis for a series expansion which compares favorably to other expansions in a lot of cases. The functions have also proven useful in channel estimation [21], wavelets [22], filter design [23], etc.

In [24] Slepian presented the discrete equivalent of the PSWF: the Discrete Prolate Spheroidal Sequence (DPSS) $\psi_{k,W}(i)$ $i = 0 \ldots L$ and $k = 0 \ldots L$ the order of the DPSS. He proved that they can be defined as the solution to a discrete energy maximization problem. As in (6), they are also the eigenvectors of a $L \times L$ sinc-matrix with elements:

$$H(L, W)_{k,l} = \frac{sin(2\pi\ W\ (k-l))}{\pi\ (k-l)} \tag{10}$$

where L is both the number of DPSSs in a set and the amount of samples per DPSS. W is a bandwidth with the constraint $0 < W < \frac{1}{2}$, resulting from the Nyquist theorem dictating that only frequencies up to half the sampling frequency can be accurately represented.

In theory it is possible to calculate the DPSSs from (10), but unfortunately the problem is ill-conditioned. Although it can be proven that the eigenvalues of (10) are all distinct, they are all concentrated around either 0 or 1, and the difference between two eigenvalues can be smaller then the numerical precision used in the calculations.

Fortunately there is, similar to (7) the PSWFs, a third way to define them by using a difference equation,

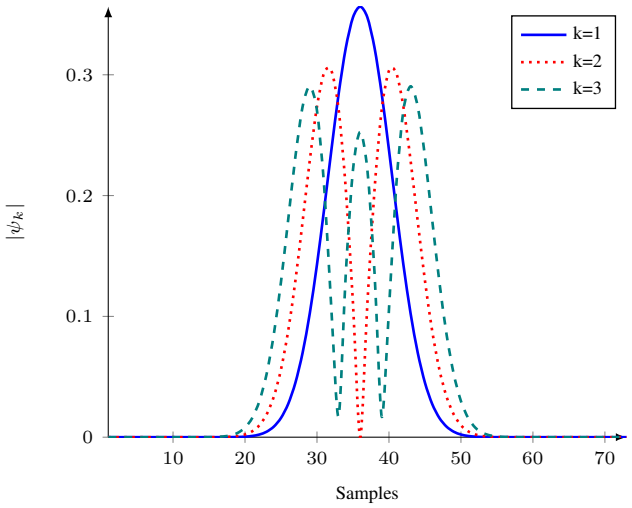

Fig. 1. Absolute value of the DPSS's with length $L = 73$

[25], [24]:

$$\frac{1}{2}k(L-k)v_{k-1} + \left[\left(\frac{L-1}{2} - k\right)^2 \cos(2\pi W) - \theta\right] v_k + \frac{1}{2}(k+1)(L-1-k)v_{k+1} = 0 \tag{11}$$

This difference equation can be written as an eigenvalue problem for the matrix $T(L, W)$, defined as follows:

$$T(L,W)_{k,l} = \begin{cases} \frac{1}{2}k(L-k) & l = k-1 \\ \left(\frac{L-1}{2} - k\right)^2 \cos(2\pi\ W) & l = k \\ \frac{1}{2}(k+1)(L-1-k) & l = k+1 \\ 0 & \text{otherwise} \end{cases} \tag{12}$$

with L and W defined as before. Because this matrix commutes with the matrix $H(L, W)$ from (10), it has the same eigenvectors, but different eigenvalues: the eigenvalues of $T(L, W)$ are not clustered, eliminating the possibility that the eigenvector problem becomes ill-conditioned. This method, which has been used in this article, provides a robust and fast numerical way to generate the DPSSs.

As for PSWFs, the DPSSs are orthonormal, $\sum_{i=0}^{L-1} \psi_{k,W}(i)\psi_{l,W}(i) = \delta_{k,l}$, and they form a complete basis for vectors of length L. Remark that no equivalent for properties (8) and (9) of the PSWFs could be found. It would be very interesting if such properties would exist, and this remains an interesting topic for further research.

In Figure 1 the magnitude of the first 3 orders of the DPSS $|\psi_k|$ is shown for a number of samples $L = 73$.

IV. Slepian Decomposition

Because the PSWFs and DPSSs are the solutions to an energy maximization problem for bandlimited functions, see (5) and (10), they are extremely well suited to model band limited signals.

The Slepian decomposition used here assumes that the radiation pattern is known at L discrete frequency

samples. The decomposition starts by expanding the radiation pattern following (1). The frequency-dependent coefficients $A_{n,m}(f) = \sum_{k=0}^{L} A_{n,m,k}\psi_k(f)$ and $B_{n,m}(f) = \sum_{k=0}^{L} B_{n,m,k}\psi_k(f)$ are expanded into a series of DPSSs, where $\psi_k(f)$ is the DPSS of order k, calculated as the eigenvector of matrix $T(L, W)$ defined by (12).

For our purpose the bandwidth parameter W is a free parameter which can be chosen to best suit the application. An optimal value for W is determined by using a particle swarm optimization algorithm, [26], which maximizes the energy contained in the first 20 orders of the Slepian expansion. The algorithm performed 3000 iterations, after which a value of $W = 0.1254$ was obtained. A value within 0.1% of the final value was obtained after 200 iterations, so it is safe to assume that the optimal value for this problem was found. If the radiation pattern is known as a continuous function of frequency, PSWFs should be taken as basis functions for the Slepian expansion.

Since the DPSSs are the natural vectors for a bandlimited series, [21], the energy of the coefficients decreases with increasing order of the Slepian modes. We can therefore truncate the series to a maximum of K coefficients without great loss of precision, by replacing L with K in both formulas. A rough value for the maximum order K can be found using the following rule of thumb:

$$K \geq \left\lceil 5\frac{f_2}{f_1} \right\rceil \tag{13}$$

where f_2 is the upper limit of the frequency band of interest and f_1 the lower limit. The final expression for the radiation pattern $\boldsymbol{F}(\phi, \theta, f)$ then becomes:

$$\boldsymbol{F}(\phi,\theta,f) = \sum_{k=0}^{K}\sum_{n=1}^{M}\sum_{m=-n}^{n} \left[A_{n,m,k}\boldsymbol{\Psi}_n^m(\phi,\theta) + B_{n,m,k}\boldsymbol{\chi}_n^m(\phi,\theta)\right]\psi_k(f) \tag{14}$$

V. Fidelity Factor

The model presented in the previous sections would have little advantages other than data compression, if the radiation pattern needs to be explicitly reconstructed to perform calculations. However UWB performance measures based on the radiation pattern can directly be calculated using the model coefficients. In this section this is shown for the fidelity factor, defined in [3].

The fidelity factor $\boldsymbol{\Phi}(\phi, \theta)$ is one of the most often used pulse-modulated-UWB performance measures, defined in [3] as follows:

$$\boldsymbol{\Phi}(\phi,\theta) = \max_{\tau}\left[\int_{-\infty}^{\infty} \hat{p}(t)\hat{\boldsymbol{r}}(\phi,\theta,t+\tau)dt\right] \tag{15}$$

where $\hat{p}(t) = \frac{p(t)}{\sqrt{\int_{-\infty}^{\infty}|p(t)|^2}}$ is the normalised version of the input pulse $p(t)$, $\hat{\boldsymbol{r}}(\phi,\theta,t) = \frac{p(t)*\boldsymbol{h}(\phi,\theta,t)}{\sqrt{\int_{-\infty}^{\infty}|p(t)*\boldsymbol{h}(\phi,\theta,t)|^2}}$ is the normalised version of the output pulse $\boldsymbol{r}(\phi, \theta, t)$ and $\boldsymbol{h}(\phi, \theta, t)$ the impulse response of the antenna. The Fourier transform of $\boldsymbol{h}(\phi, \theta, t)$, i.e. the frequency response $\boldsymbol{H}(\phi, \theta, f)$, is given by the radiation pattern $\boldsymbol{F}(\phi, \theta, f)$ of the antenna. Knowledge of the radiation pattern over all angles as a function of frequency and the input-pulse as a function of time is necessary to compute the fidelity factor.

Making use of the definitions of $\hat{\boldsymbol{r}}(\phi,\theta,t)$ and $\hat{p}(t)$, (15) becomes:

$$\boldsymbol{\Phi}(\phi,\theta)=\max_{\tau}\left[\frac{IFT\left[P(f)P^{*}(f)\boldsymbol{H}^{*}(\phi,\theta,f)\right]}{\sqrt{\int\limits_{-\infty}^{\infty}\left|P(f)\right|^{2}df}\sqrt{\int\limits_{-\infty}^{\infty}\left|P(f)\boldsymbol{H}(\phi,\theta,f)\right|^{2}df}}\right] \tag{16}$$

where the correlation is calculated in the frequency domain, $IFT()$ denotes the inverse Fourier transform of its arguments, the superscript * stands for the complex conjugate and the denominator has been calculated using Parceval's theorem. Substituting (14) in (16) results after some simplifications in:

$$\boldsymbol{\Phi}(\phi,\theta)=\max_{\tau}\left[\frac{\sum\limits_{k=0}^{k}\alpha_{k}(\tau)\boldsymbol{\beta}_{k}(\phi,\theta)}{\sqrt{\int\limits_{-\infty}^{\infty}\left|P(f)\right|^{2}df}\sqrt{\int\limits_{-\infty}^{\infty}\left|\sum\limits_{k=0}^{K}\alpha_{k}(\tau)\boldsymbol{\beta}_{k}(\phi,\theta)\right|^{2}d\tau}}\right] \tag{17}$$

where $\alpha_k(\tau)$

$$\alpha_{k}(\tau)=IFT\left[\left|P(f)\right|^{2}\psi_{k}(f)\right] \tag{18}$$

only depends on the input pulse and $\boldsymbol{\beta}_k(\phi,\theta)$

$$\boldsymbol{\beta_{k}}(\phi,\theta)=\sum_{n=0}^{M}\sum_{m=-n}^{n}A_{n,m,k}\boldsymbol{\Psi}_{n}^{m}(\phi,\theta)+B_{n,m,k}\boldsymbol{\chi}_{n}^{m}(\phi,\theta) \tag{19}$$

only depends on the antenna radiation pattern. The effects of the antenna and the input pulse are clearly separated. This property is a great advantage during optimizations as only $\alpha_k(\tau)$ or $\boldsymbol{\beta}_k(\phi,\theta)$ needs to be calculated in each run, respectively depending on whether the antenna or input pulse are being optimized. (17) expresses the fidelity factor as a function of the model coefficients $A_{n,m,k}$ and $B_{n,m,k}$ without explicitly reconstructing the entire radiation pattern, which makes the fidelity factor as a function of (ϕ,θ) easier to calculate because a much smaller number of samples needs to be evaluated.

Despite the fact that the definition of the fidelity factor (15) depends on (ϕ,θ), most papers, such as [27] and even the original paper by Lamensdorf and Susman [3], present one fidelity factor for the entire antenna, along a single angle of departure. It is measured by correlating the input pulse with the output pulse of the entire *system*, where all other elements of the system except for the Antenna Under Test are assumed distortionless. This approach only yields useful results for highly directive antennas, which have one well-defined direction of radiation, along which the fidelity factor is calculated. However, most UWB antennas are meant for mobile use and have rather omnidirectional radiation patterns, as the locations of the transmitting and receiving antenna are not fixed. More recent papers, such as [28], recognize this flaw and evaluate the fidelity factor for a few different directions. Here the fidelity factor is for the first time evaluated for all angles (ϕ,θ).

VI. Singularity Expansion Method

To validate the Slepian mode expansion we will also consider the frequently used singularity expansion method, [29], which can be computed by Prony's method [30], [31], [32] or the matrix pencil method (MPM) [33]. In antenna modeling the MPM is often used because of its robustness and computational efficiency: [34]

uses the MPM to model the impulse response of an antenna in *one* direction. [35] is similar to [34] but models the effective length instead of the antenna transfer function.

A modified version of the MPM is proposed in [36] to model the radiation pattern for multiple directions. [37] applies this algorithm together with a spherical wave decomposition to model an antenna radiation pattern in multiple directions. The SEM expansion for one polarisation and multiple directions looks as follows:

$$y(\phi,\theta,t) = \sum_{p=1}^{P} R_p(\phi,\theta)\exp(s_p t) \tag{20}$$

where P is theoretically ∞, but can be truncated to a finite number with minimal loss in accuracy because of the bandlimited character of antennas. The poles s_p are the natural frequencies of the object and are theoretically independent of the direction of observation. Unfortunately, because of noise and inaccuracies, in both simulation and measurements, the resulting poles will differ for different look directions. This is why a separate algorithm to calculate the poles for multiple directions, such as the one presented in [36], is needed. It should be noted that the extraction of the poles revolves around an SVD expansion of a matrix that grows linearly with the number of directions used in the expansion. For this reason the poles are calculated using a 2D cut of the radiation pattern, after which these poles are used to calculate the residues for the entire 3D radiation pattern.

Once the poles s_p and residues $R_p(\phi,\theta)$ are known, the angular dependencies of the residues can be decomposed into spherical waves, using the same approach outlined in Section II, where the residues of both components of the radiation pattern are recombined as a vector:

$$\boldsymbol{R_p}(\phi,\theta) = \sum_{n=1}^{M}\sum_{m=-n}^{n} A_{n,m,p}\boldsymbol{\Psi}_n^m(\phi,\theta) + B_{n,m,p}\boldsymbol{\chi}_n^m(\phi,\theta) \tag{21}$$

Because the SEM is a form of rational modeling, it is very sensitive to discontinuities, such as noise, in the dataset. It is therefore important to start with the SEM decomposition before decomposing the angular dependencies of the residues into spherical wave functions. The spherical wave decomposition will have a lot of coefficients with a very low energy level and thus a very significant noise contribution. These coefficients will make it much more difficult for the SEM to find the correct antenna poles, greatly reducing the accuracy of the model.

VII. Validation

A. Flexible UWB Antenna

The model proposed in this paper is now validated based on an in house developed UWB antenna for use in the 3.1 GHz to 10.6 GHz FCC band. The antenna uses the popular planar monopole topology, amongst others also used in [38], with an inverted tear top-element. This topology has numerous advantages. Its planar nature and small size allow the antenna to be easily integrated into other devices, it offers a very large bandwidth and has a small group delay.

The antenna was fabricated on a flexible polyimide substrate, consisting of a $25\mu m$ polyimide layer and a $18\mu m$ copper layer. The polyimide has a dielectric constant of $\epsilon_r = 3.2$ at 10 kHz. Because the substrate is extremely thin, the exact ϵ_r in the frequency band will be of little importance. The flexibility and extremely thin nature of the antenna allows it to be very easily integrated in, for example, modern cell phones with strange form factors.

A schematic representation of the antenna is shown in Figure 2. The produced antenna is shown in Figure 3. The antenna was designed and optimised for a minimal reflection coefficient in the frequency band of interest using ADS Momentum. The corresponding dimensions are shown in Table I. The results were later verified by simulating the design in CST Microwave studio. Figure 4 shows both the simulated and measured

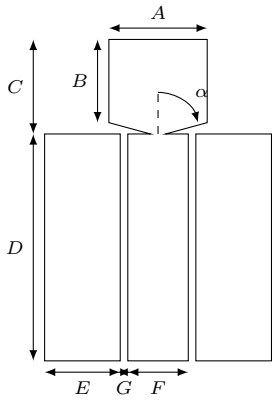

Fig. 2. Planar Monopole topology

Parameter	Value [mm]
A	18.7448
B	13.556
C	16.8549
D	29.2885
E	14.7153
F	5.3156
G	0.2
α	68°

TABLE I
ANTENNA DIMENSIONS

reflection coefficient. It can be seen that the measured and simulated curves show a good agreement: they have roughly the same shape, but the curve of the measured antenna has shifted to higher frequencies. The simulated antenna has a reflection coefficient $|S_{11}| < -10$ dB in the entire FCC band. The differences between the simulated and measured antenna are due to imperfections in the manual soldering of the SMA connector. The antenna is very sensitive to small misalignments between antenna and connector.

Fig. 3. Produced Planar Monopole Antenna

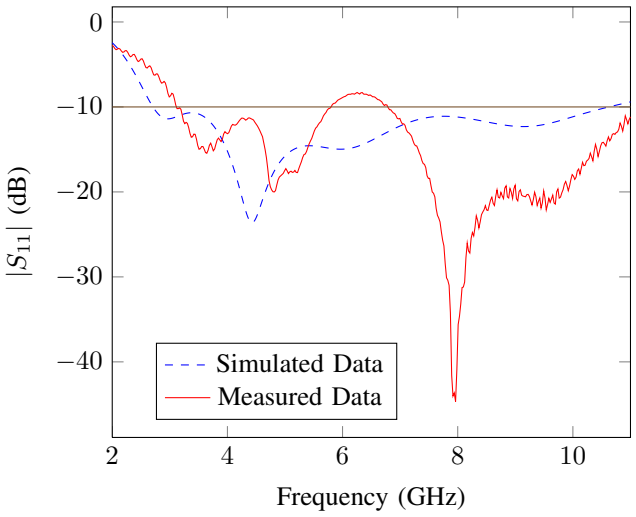

Fig. 4. Simulated and Measured Reflection Coefficient

Figures 5 and 6 show two cuts of the simulated radiation pattern as a function of frequency, for the θ and ϕ polarisation respectively. Figure 7 shows the measured radiation pattern for a fixed elevation angle $\theta = 90°$, with 121 ϕ and 51 frequency samples. The measured radiation pattern has roughly the same shape as the simulated pattern, but the noise added by the measurement makes a direct comparison impossible, especially at the higher frequencies.

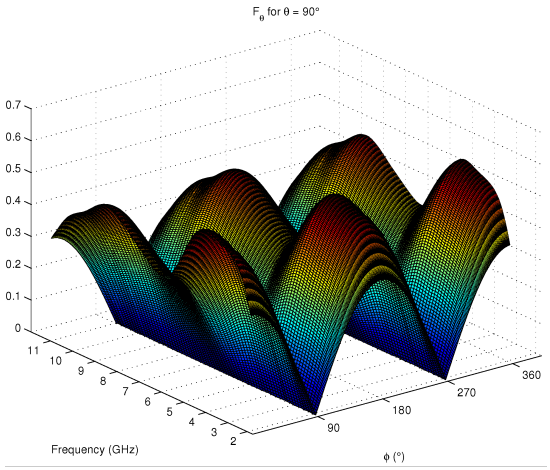

Fig. 5. F_θ simulated for $\theta = 90°$

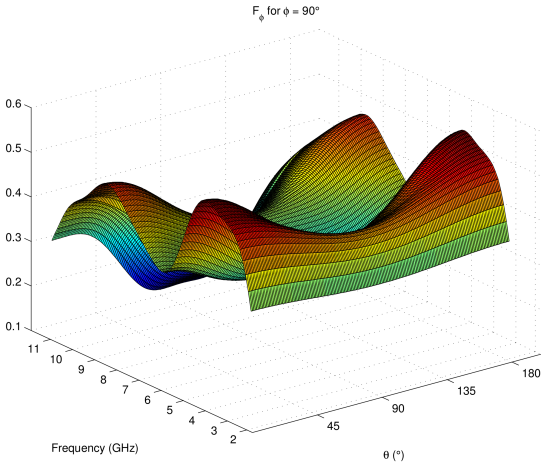

Fig. 6. F_ϕ simulated for $\phi = 90°$

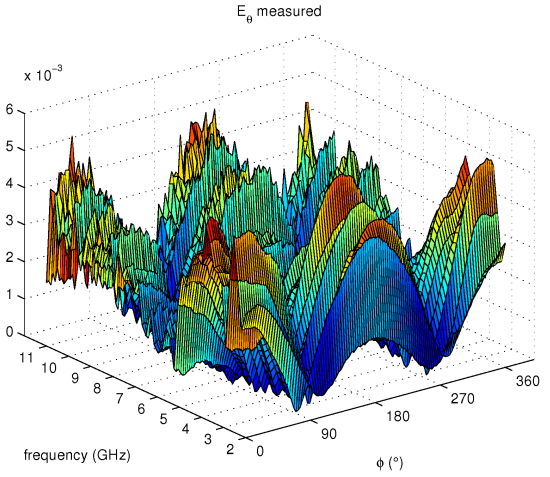

Fig. 7. F_θ measured for $\theta = 90°$

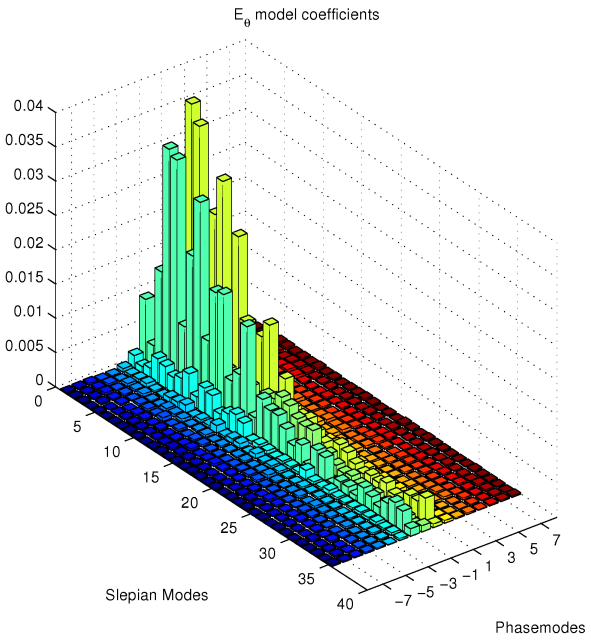

Fig. 8. Coefficients of the measured 2D radiation pattern

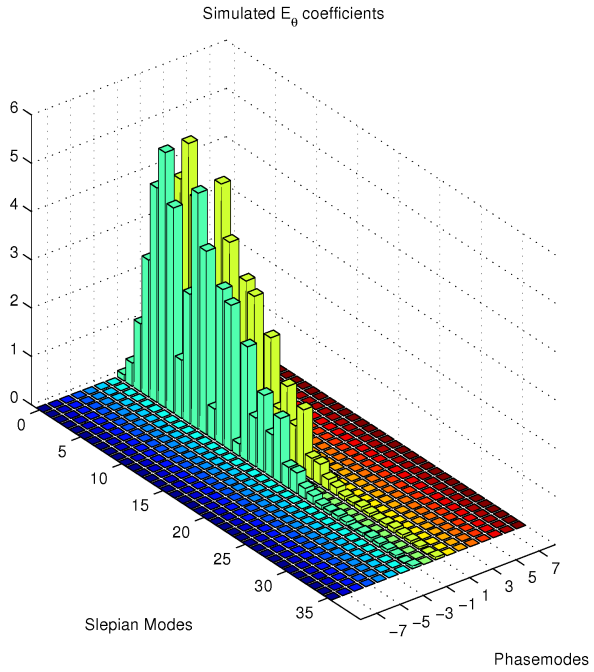

Fig. 9. Coefficients of the simulated 2D radiation pattern

B. Noise Reduction

As a first application of the new expansion proposed in this paper, we show that noise can be removed just by neglecting the higher order (spherical) phase modes and/or Slepian modes. Figure 7 presents a 2D cut of the radiation pattern. Here the angular dependency of this radiation pattern is modeled using phase modes in azimuth only instead of a complete vector spherical expansion. The model coefficients are shown in Figure 8 for the measured data and in Figure 9 for the simulated data. Despite the considerable noise contribution at higher frequencies, the energy of the coefficients still decreases exponentially with increasing order. The noise in the measurement is visible by the increased noise floor in the coefficient data.

Figure 10 shows the reconstructed radiation pattern. It has good resemblance with the original measured data, but a greatly reduced noise contribution. Truncating the Slepian series and phase modes kept the frequency dependency of the radiation pattern but filtered out the measurement noise. The model is, unlike rational modeling methods, so resistant to noise that it can effectively be used as a filter.

C. Data Compression

Next the model constructed in Section IV is applied to the simulated full 3D radiation pattern of the antenna from Section VII-A using Matlab R2007b. The radiation pattern is sampled every degree for both the azimuth angle ϕ and elevation angle θ for both polarisations. The radiation pattern was sampled every 125 MHz. This results in a radiation pattern described by 2x73x360x180 samples.

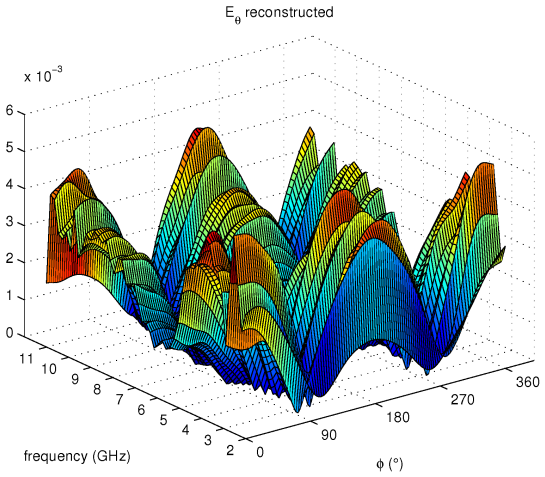

Fig. 10. Reconstructed Measured Radiation Pattern

1) Slepian expansion: The parameters of the model were chosen to be $M = 8$ and $K = 29$. This choice results in a model of 2 coefficient cubes with each 30x8x17 samples, a reduction with a factor of more than 1159. The amount of samples can be reduced even further by taking into account that no vector spherical modes exist for $|m| \geq n$.

Since showing two 3D cubes of data is not practical, 3 cuts of one cube will be shown: Figure 11 shows the $A_{n,m,k}$ cube for a fixed Slepian Mode order, $k = 1$, Figure 12 shows the $A_{n,m,k}$ cube for a fixed phase mode, $m = 3$, and Figure 13 shows the $A_{n,m,k}$ cube for a fixed n value, $n = 6$. It can be visually verified that the energy of the coefficients has become sufficiently low at the truncation boundaries.

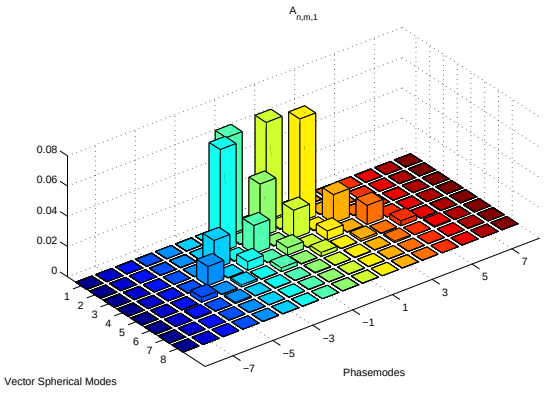

Fig. 11. Fixed Slepian Mode Cut: $A_{n,m,k}$ for $k = 1$

The the relative error between the original sampled radiation pattern and the radiation pattern reconstructed

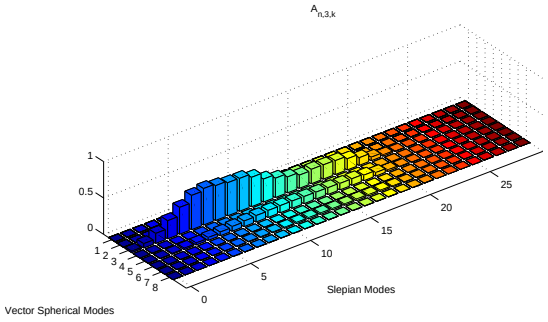

Fig. 12. Fixed Phasemode Cut: $A_{n,m,k}$ for $m = 3$

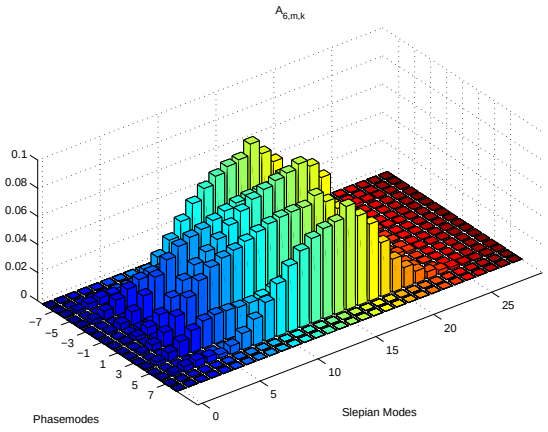

Fig. 13. Fixed Vector Spherical Mode Cut: $A_{n,m,k}$ for $n = 6$

from the model coefficients for a given polarisation is evaluated using the following error function:

$$Error = \frac{\sum_{\phi}\sum_{\theta} |F_{orig}(\phi,\theta,f) - F_{recon}(\phi,\theta,f)|^2}{\sum_{\phi}\sum_{\theta} |F_{orig}(\phi,\theta,f)|^2} \tag{22}$$

where $F_{orig}(\phi,\theta,f)$ and $F_{recon}(\phi,\theta,f)$ denote the original and reconstructed radiation pattern, respectively. Figure 14 shows the relative error for both polarisations. The two relative errors remain smaller than 2%. Both errors are almost equal because the information for both polarisations is present in equal amounts in the $A_{m,n,k}$ and $B_{m,n,k}$ coefficients: leaving out the higher order coefficients affects both polarisations at the same time in the same way.

2) SEM expansion: For validation the SEM model from Section VI is used to model the same radiation pattern. Because the SEM expansion performs a SVD expansion there is a limit to the size of the matrix used in the model. For this reason the radiation pattern is sampled every 3 degrees instead of every single degree. Combined with a frequency sampling every 125 MHz, this results in a radiation pattern of 2x73x120x60 samples.

The SEM expansion has another major drawback: it can only model reasonably smooth data. This is in general not a problem for simulated antenna radiation patterns, except when the radiation pattern contains a very steep

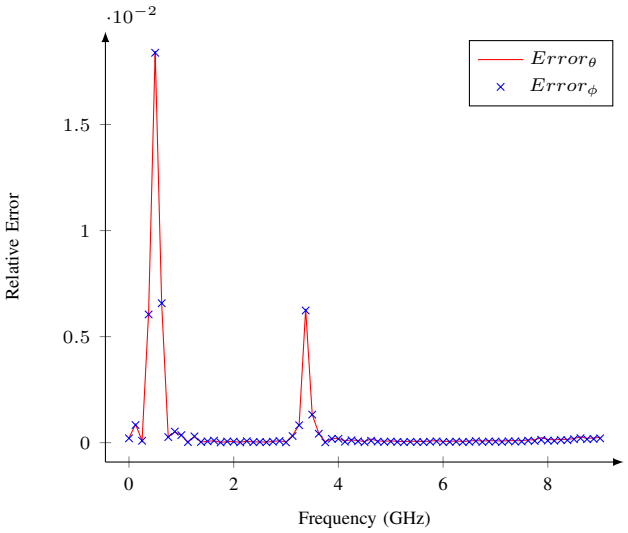

Fig. 14. Relative Error for both polarisations

null. The ϕ-polarisation of the radiation pattern contains a zero that is not smooth over frequency, due to numerical noise in the simulations. The very small values are very noisy as a function of frequency, but are continuous as a function of the angle θ. Because of this reason the SEM expansion can not model the ϕ-polarisation of the radiation pattern and in what follows only the θ-polarisation is considered.

The parameters of the vector spherical expansion in the SEM procedure are chosen in the same way as in the Slepian expansion procedure: $M = 15$. At this point the energy contained in the vector spherical modes has decreased sufficiently to neglect the higher order modes. The number of poles to be included in the SEM expansion was determined by trial and error: the number of poles was increased until the radiation pattern could be reasonable well reconstructed. This results in a number of poles $P = 35$. It should also be noted that the reconstruction error decreases very steeply when the number of poles increases: the reconstructed radiation pattern looks nothing like the original radiation pattern when only 34 poles are used. This behaviour renders the SEM expansion useless for filtering purposes. The model now contains 2x(35x31x15+35) or 32620 coefficients. This is a reduction by a factor 32.

Figure 15 displays a cut of the coefficient cube for a fixed pole: $p = 3$. We can clearly see that the energy contained in the residues can still be accurately modeled with a spherical wave expansion: the energy of the coefficients exponentially decreases when the orders m and n increase. Figure 16 displays the coefficient cube for a fixed order $m = 3$. The energy vector spherical modes still decreases exponentially with increasing order n. The energy in the coefficients does not decrease when the order of the poles increases, but this is not a problem, as the energy of the residues is plotted and the actual frequency dependency is modeled in the poles. Figure 17 shows the poles for the θ-polarisation by means of a scatter plot in the complex plane.

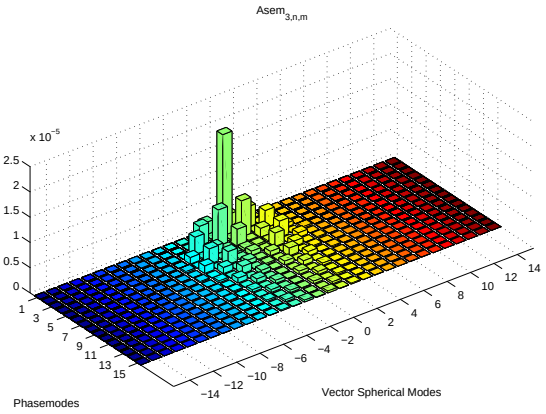

Fig. 15. Fixed Pole Cut: $Asem_{p,n,m}$ for $p = 3$

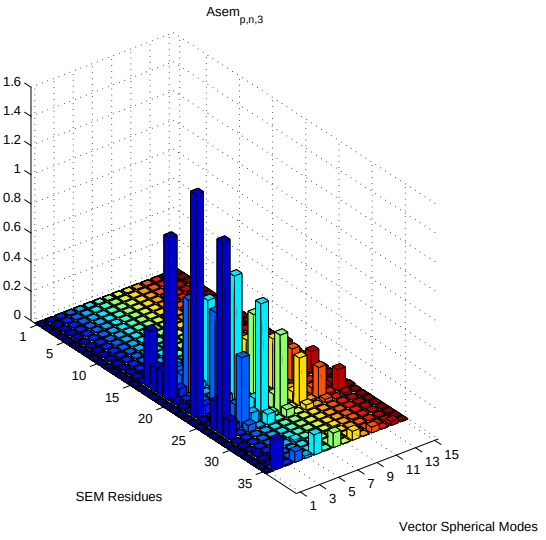

Fig. 16. Fixed Phasemode Cut: $Asem_{p,n,m}$ for $m = 3$

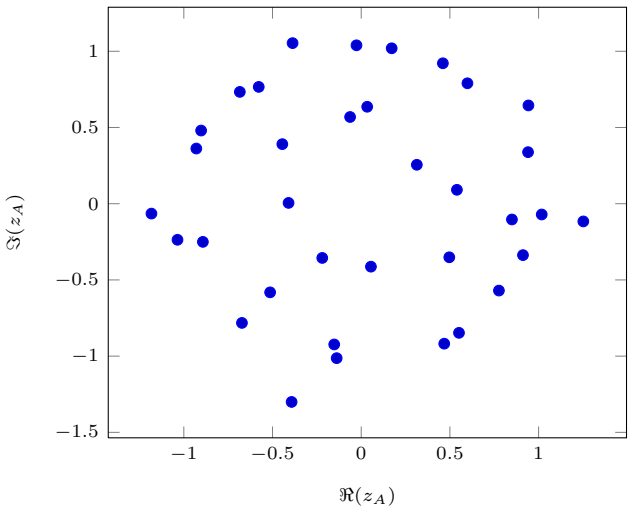

Fig. 17. Poles of the θ polarisation

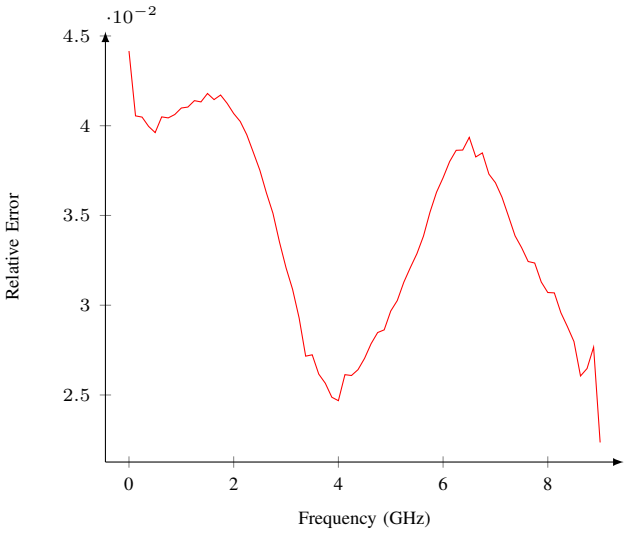

Fig. 18. Relative Error for E_θ using SEM expansion

To compare the relative error between the reconstructed radiation pattern and the original radiation pattern, the same error function (22) is used. Figure 18 shows the relative error on E_θ. The error varies evenly over frequency with a maximum of $\approx 4.5\%$

The calculation times are compared on a quad core linux system (two dual core AMD Opteron$^{\text{tm}}$ processors model 270 with 2GHz per core and 8 GB of RAM) using Matlab, by executing each algorithm 100 times on a 2x73x120x60 radiation pattern and taking the mean calculation time. It takes on average 0.1846 seconds to calculate the Slepian model coefficients for a radiation pattern of this size and 29.7265 seconds to expand the radiation pattern in SEM coefficients.

D. Fidelity Factor Evaluation

As a third application, the fidelity factor, defined in (15), was calculated using a fifth-order derivative of a Gaussian monocycle, which is known to fit into the FCC spectral mask, [39]:

$$P(t) = A\left(-\frac{t^5}{\sqrt{2\pi}\sigma^{11}} + \frac{10t^3}{\sqrt{2\pi}\sigma^{9}} - \frac{15t}{\sqrt{2\pi}\sigma^{7}}\right)\exp\left(-\frac{t^2}{2\sigma^2}\right) \tag{23}$$

where A is a normalisation constant to fit the pulse to the FCC spectral mask, and $\sigma = 51$ps. The FCC compliant pulse is shown in Figure 19. Figure 20 shows the spectrum of the pulse and the FCC spectral mask for indoor UWB communications.

The fidelity factor will not be evaluated at the locations of the nulls in the radiation pattern. The fidelity factor suffers from the fact that it is only defined for a single polarisation and that a null in the radiation pattern deteriorates the fidelity factor significantly, even though these directions do not contribute to the radiation. For Φ_θ these directions are $\theta = 0°$ and $\theta = 90°$, for Φ_ϕ these directions are $\phi = 0°$ and $\phi = 180°$. The fidelity factors for all other angles ϕ and θ and both polarisations, calculated using direct application of (15) are shown in Figure 21 and Figure 22.

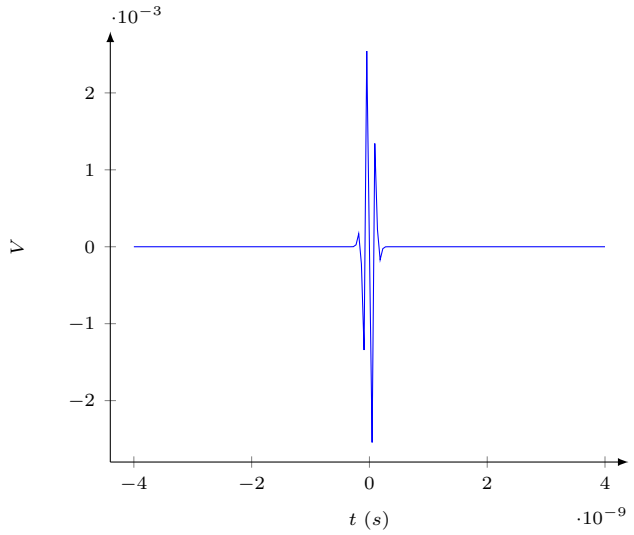

Fig. 19. FCC compliant UWB pulse

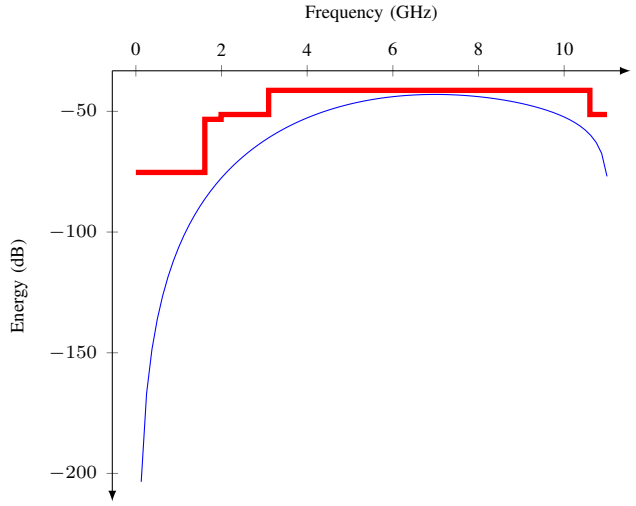

Fig. 20. UWB pulse spectrum and FCC spectral mask

The fidelity factor $\mathbf{\Phi}(\phi, \theta)$ is larger than 0.8 for most of the directions and is 0.94 in the main radiation direction for both polarisations. These are good results: the maximum value of $\mathbf{\Phi}(\phi, \theta)$ compares well to the results presented in [28], and especially the ϕ-component of $\Phi(\phi, \theta)$ only varies by a small amount as a function of (ϕ, θ). It can also be seen that the antenna performs a lot better for ϕ-polarisation than for θ-polarisation: $\Phi_\theta(\phi, \theta)$ is very low for a few ϕ angles. If only the system fidelity factor, or the fidelity factor at 5 discrete directions, had been evaluated, these directions with high distortion would not have been known.

The fidelity factor is now evaluated using the Slepian model, using (17). Figure 23 shows the relative error between the original θ-polarised fidelity factor and the one calculated using the Slepian model. Figure 24 shows the relative error for the ϕ-polarisation fidelity factor. The relative error is well below 1% for both

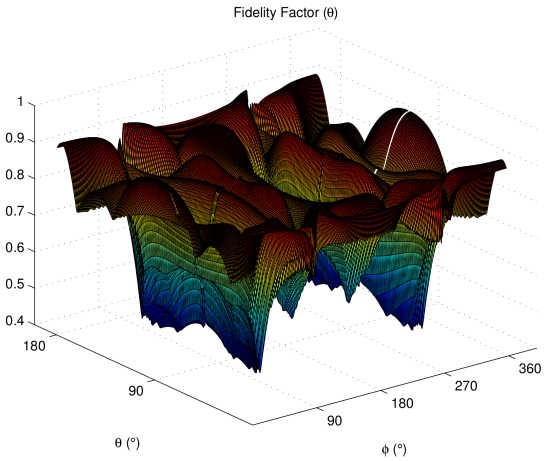

Fig. 21. Fidelity Factor $\mathbf{\Phi}(\phi, \theta)$ for the θ polarisation

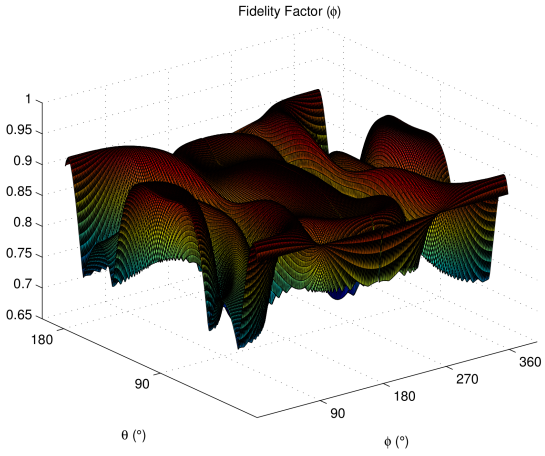

Fig. 22. Fidelity Factor $\mathbf{\Phi}(\phi, \theta)$ for the ϕ polarisation

polarisations. The peaks in both figures are located near the nulls of the radiation pattern: the radiated energy in these directions is smaller which means that the error made by the model becomes relatively larger.

Figure 25 shows the relative error on F_θ calculated from the SEM decomposition. We notice that the error is of the same magnitude as the error made on the radiation pattern itself: 4%.

We now compare the computation speed of the direct algorithm, based on the definition of the fidelity factor (15), which evaluates the correlations and convolutions in the frequency domain using the convolution theorem of the DFT, with the method based on the Slepian expansion, using (17). The direct method requires a CPU-time of 52.67s. The method using model coefficients takes 10.37s to calculate a fidelity factor for all directions (ϕ, θ). This time includes the decomposition of the complete frequency-dependent 3D radiation pattern into coefficients $(A_{m,n,k}, B_{m,n,k})$. Using the new compact model, the fidelity factor can be calculated roughly five times faster, which is a considerable increase in performance.

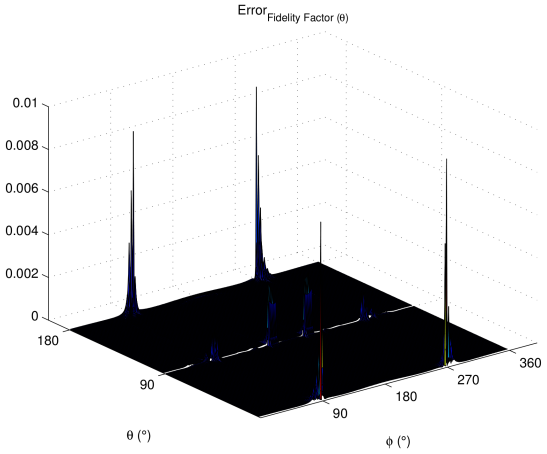

Fig. 23. Relative Error for the θ-polarisation Fidelity Factor

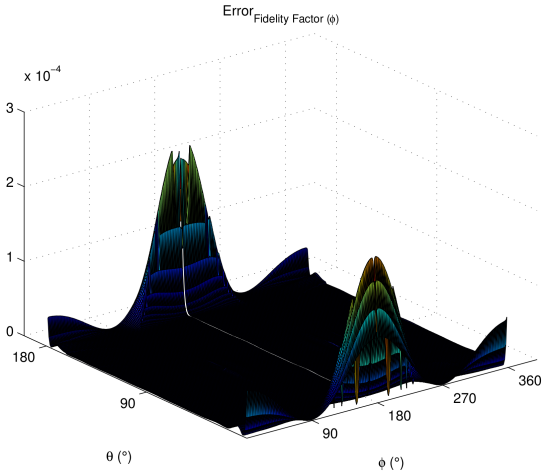

Fig. 24. Relative Error for the ϕ-polarisation Fidelity Factor

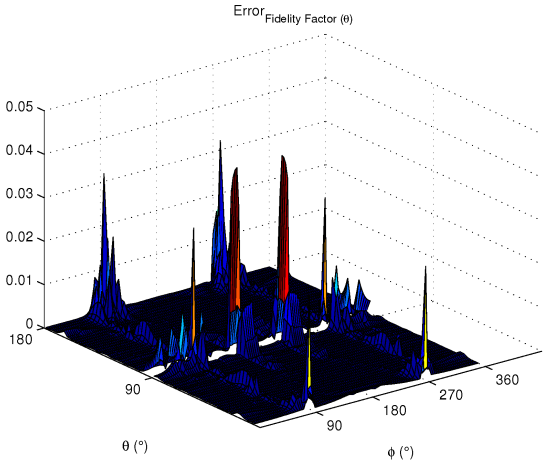

Fig. 25. Relative error on the Fidelity Factor for the θ-polarisation

E. Comparison

The comparison between the two models yields the following observations:

1) The Slepian expansion can handle much larger datasets than the SEM expansion
2) The SEM expansion is very sensitive to noise: it is unable to model the ϕ-polarisation which contains a deep null. The Slepian expansion handles this without problems.
3) The Slepian expansion modeled a 2x73x360x180 radiation pattern by means of 2x30x17x8 coefficients with a maximum relative error smaller than 2%. The SEM expansion modeled a 2x73x120x60 using 2x35x31x15+35 coefficients with a maximum relative error smaller than 4.5%. This means that the Slepian expansion modeled a more detailed radiation pattern with less coefficients and greater accuracy.
4) The Slepian expansion modeled the radiation pattern on average in 0.1846 seconds. The SEM expansion in 29.7265 seconds. For a given dataset the Slepian expansion is roughly a factor 161 faster.

VIII. Conclusion

In this paper a novel model to describe the radiation pattern of wideband antennas, using vector spherical wave functions and discrete prolate spheroidal sequences, was proposed. This model compresses a radiation pattern with a factor of more than 1159, while having a relative error smaller than 2%. The model has also been used to evaluate the fidelity factor $\mathbf{\Phi}(\phi, \theta)$ for the first time for all angles (ϕ, θ). Using the model, the fidelity factor $\mathbf{\Phi}(\phi, \theta)$ is evaluated a factor 5 faster, with a relative error smaller than 1%. Modeling a measured 2D cut of the radiation pattern shows that the model is also very noise resistant and can be used to filter out measurement noise. The model was also compared to a model based on the often used SEM expansion. The Slepian model suffers from none of the known drawbacks of the SEM expansion, is faster to evaluate and models the radiation pattern more accurately with less coefficients.

References

[1] "New public safety applications and broadband internet access among uses envisioned by FCC authorization of ultra-wideband technology-FCC news release 2002 [online]." http://www.fcc.gov/Bureaus/Engineering_Technology/News_Releases/2002/nret0203.html. [Online]. Available: http://ftp.fcc.Gov/Bureaus/Engineering_Technology/News_Releases/2002/nret0203.pdf

[2] W. Lauber and S. Palaninathan, "Ultra-wideband antenna characteristics and pulse distortion measurements," in *Ultra-Wideband, The 2006 IEEE 2006 International Conference on*, 2006, pp. 617–622.

[3] D. Lamensdorf and L. Susman, "Baseband-pulse-antenna techniques," *IEEE Antennas and Propagation Magazine*, vol. 36, no. 1, pp. 20–30, Feb. 1994, definition of the Fidelity Factor.

[4] D.-H. Kwon, "Effect of antenna gain and group delay variations on pulse-preserving capabilities of ultrawideband antennas," *IEEE Transactions On Antennas and Propagation*, vol. 54, no. 8, pp. 2208–2215, Aug. 2006.

[5] J. McLean, H. Foltz, and R. Sutton, "Pattern descriptors for uwb antennas," *IEEE Transactions on Antennas and Propagation*, vol. 53, no. 1, pp. 553–559, Jan. 2005.

[6] T. Dissanayake and K. P. Esselle, "Correlation-based pattern stability analysis and a figure of merit for UWB antennas," *IEEE Transactions on Antennas and Propagation*, vol. 54, no. 11, pp. 3184–3191, Nov. 2006.

[7] H. Rogier and E. Bonek, "Analytical spherical-mode-based compensation of mutual coupling in uniform circular arrays for direction-of-arrival estimation," *Archiv fur Elektronik und Übertragungstechnik (AEÜ)-International Journal of Electronics and Communications*, vol. 60, no. 3, pp. 179–189, March 2006.

[8] H. Xiao, V. Rokhlin, and N. Yarvin, "Prolate spheroidal wavefunctions, quadrature and interpolation," *Inverse Problems*, vol. 17, pp. 805–838, aug 2001. [Online]. Available: http://adsabs.harvard.edu/abs/2001InvPr..17..805X

[9] D. H. Werner and R. J. Allard, "The simultaneous interpolation of antenna radiation patterns in both the spatial and frequency domains using model-based parameter estimation," vol. 48, no. 3, pp. 383–392, March 2000.

[10] D. E. N. Davies, *The Handbook of Antenna Design: A. Rudge, K. Milne, A. Olver and P. Knight, Eds.*, ser. IEE Electromagnetic Wave Series. London: Peregrinus, 1983, ch. 12.

[11] R. F. Harrington, *Time-Harmonic Electromagnetic Fields*, ser. Electrical and Electronic Engineering Series. New York: McGraw-Hill, 1961.

[12] O. Bucci, G. D'Elia, G. Franceschetti, and R. Pierri, "Efficient computation of the far field of parabolic reflectors by pseudo-sampling algorithm," *IEEE Transactions on Antennas and Propagation*, vol. 31, no. 6, pp. 931–937, Nov 1983.

[13] H. Rogier, "Spatial correlation in uniform circular arrays based on a spherical-waves model for mutual coupling," *Archiv fur Elektronik und Übertragungstechnik (AEÜ)-International Journal of Electronics and Communications*, vol. 60, no. 7, pp. 521–532, March 2006.

[14] C. Roblin and A. Sibille, "Ultra compressed parametric modeling of UWB antenna measurements using symmetries," in *XXIX URSI General Assembly*, Chicago, August 2008.

[15] D. Slepian, "Some comments on fourier analysis, uncertainty and modeling," *SIAM Review*, vol. 25, no. 3, pp. 379–393, 1983. [Online]. Available: http://www.jstor.org/stable/2029386

[16] D. Slepian and H.O.Pollak, "Prolate spheroidal wave functions, fourier analysis, and uncertainty - i," *Bell Systems Technology Journal*, vol. 40, no. 1, pp. 43–64, jan 1961.

[17] H. Landau and H. Pollak, "Prolate spheroidal wave functions, fourier analysis, and uncertainty - ii," *Bell Systems Technology Journal*, vol. 40, no. 1, pp. 65–84, jan 1961.

[18] ——, "Prolate spheroidal wave functions, fourier analysis and uncertainty - iii," *Bell Systems Technology Journal*, vol. 41, no. 4, pp. 1295–1336, july 1962.

[19] D. Slepian, "Prolate spheroidal wave functions, fourier analysis and uncertainty - iv," *Bell Systems Technology Journal*, vol. 43, no. 6, pp. 3009–3058, November 1964.

[20] I. C. Moore and M. Cada, "Prolate spheroidal wave functions, an introduction to the slepian series and its properties," *Appl. Comput. Harmon. Anal.*, vol. 16, pp. 208–230, 2004.

[21] T. Zemen and C. Mecklenbrauker, "Time-variant channel estimation using discrete prolate spheroidal sequences," *IEEE Transactions on Signal Processing*, vol. 53, no. 9, pp. 3597–3607, Sept. 2005.

[22] G. G. Walter and X. Shen, "Wavelets based on prolate spheroidal wave functions," *J. Fourier Anal. Appl.The Journal of Fourier Analysis and Applications*, vol. 10, no. 1, pp. 1–26, 2004.

[23] L. Varshney, "On the use of discrete prolate spheroidal windows for frequency selective filter design," *Applications of Signal Processing*, feb 2004.

[24] D. Slepian, "Prolate spheroidal wave functions, fourier analysis, and uncertainty. v - the discrete case," *AT T Technical Journal*, vol. 57, pp. 1371–1430, jun 1978.

[25] F. A. Grünbaum, "Eigenvectors of a toeplitz matrix: Discrete version of the prolate spheroidal wave functions," *SIAM Journal on Algebraic and Discrete Methods*, vol. 2, no. 2, pp. 136–141, 1981. [Online]. Available: http://link.aip.org/link/?SML/2/136/1

[26] P. Demarcke, H. Rogier, R. Goossens, and P. De Jaeger, "Beamforming in the presence of mutual coupling based on constrained particle swarm optimization," *IEEE Transactions on Antennas and Propagation*, vol. 57, no. 6, pp. 1655–1666, June 2009.

[27] A. Abbosh and M. Bialkowski, "A UWB directional antenna for microwave imaging applications," in *Proc. IEEE Antennas and Propagation International Symposium*, 9–15 June 2007, pp. 5709–5712.

[28] R. Aylo, K. Kabalan, A. El-Hajj, M. Al-Husseini, and J. Costantine, "An investigation of the wideband properties of a resistively-loaded v-shaped conical antenna," in *Proc. IEEE Antennas and Propagation Society International Symposium AP-S 2008*, 2008, pp. 1–4.

[29] C. E. Baum, "On the singularity expansion method for the solution of electromagnetic interaction problems," *EMP Interaction Note 8*, vol. 8, p. 112, DEC 1971. [Online]. Available: http://handle.dtic.mil/100.2/ADA066905

[30] B. G. R. de Prony, "Essai xperimental et analytique: sur les lois de la dilatabilit de fluides lastique et sur celles de la force expansive de la vapeur de l'alkool, diffrentes tempratures," *Journal de l'cole Polytechnique*, vol. 1, no. 22, pp. 24–76, 1795.

[31] F. Hildebrand, *Introduction to numerical analysis*, 1974. [Online]. Available: http://sfxit.ugent.be/sfx_local?sid=google;auinit=FB;aulast=Hildebrand;title=Introduction%20to%20numerical%20analysis;genre=book;isbn=0486653633;date=1974

[32] M. L. Van Blaricum and R. Mittra, "Problems and solutions associated with prony's method for processing transient data," *IEEE Transactions on Electromagnetic Compatibility*, no. 1, pp. 174–182, Part I,&eb. 1978.

[33] T. K. Sarkar and O. Pereira, "Using the matrix pencil method to estimate the parameters of a sum of complex exponentials," *IEEE Antennas and Propagation Magazine*, vol. 37, no. 1, pp. 48–55, Feb. 1995.

[34] Y. Duroc, T. P. Vuong, and S. Tedjini, "Realistic modeling of antennas for ultra wide band systems," in *Proc. IEEE Radio and Wireless Symposium*, 17–19 Oct. 2006, pp. 347–350.

[35] S. Licul and W. A. Davis, "Unified frequency and time-domain antenna modeling and characterization," *IEEE Transactions on Antennas and Propagation*, vol. 53, no. 9, pp. 2882–2888, Sept. 2005.

[36] T. K. Sarkar, S. Park, J. Koh, and S. M. Rao, "Application of the matrix pencil method for estimating the sem (singularity expansion method) poles of source-free transient responses from multiple look directions," *IEEE Transactions on Antennas and Propagation*, vol. 48, no. 4, pp. 612–618, April 2000.

[37] C. Roblin, "Ultra compressed parametric modelling of UWB antenna measurements," in *Proc. First European Conference on Antennas and Propagation EuCAP 2006*, 6–10 Nov. 2006, pp. 1–8.

[38] G. Brzezina, L. Roy, and L. MacEachern, "Planar antennas in LTCC technology with transceiver integration capability for ultra-wideband applications," *IEEE Transactions On Microwave Theory and Techniques*, vol. 54, no. 6, pp. 2830–2839, Jun. 2006.

[39] H. Sheng, P. Orlik, A. Haimovich, J. Cimini, L.J., and J. Zhang, "On the spectral and power requirements for ultra-wideband transmission," in *Proc. IEEE International Conference on Communications ICC '03*, vol. 1, 11–15 May 2003, pp. 738–742.